Tropical Cyclone Simulation and Response to CO_2 Doubling in the GFDL CM2.5 High-Resolution Coupled Climate Model

HYEONG-SEOG KIM*

NOAA/Geophysical Fluid Dynamics Laboratory, and Department of Atmospheric and Oceanic Sciences, Princeton University, Princeton, New Jersey, and Willis Research Network, London, United Kingdom

GABRIEL A. VECCHI, THOMAS R. KNUTSON, WHIT G. ANDERSON, THOMAS L. DELWORTH, ANTHONY ROSATI, AND FANRONG ZENG

NOAA/Geophysical Fluid Dynamics Laboratory, Princeton, New Jersey

MING ZHAO

NOAA/Geophysical Fluid Dynamics Laboratory, Princeton, New Jersey, and University Corporation for Atmospheric Research, Boulder, Colorado

(Manuscript received 26 July 2013, in final form 7 July 2014)

ABSTRACT

Global tropical cyclone (TC) activity is simulated by the Geophysical Fluid Dynamics Laboratory (GFDL) Climate Model, version 2.5 (CM2.5), which is a fully coupled global climate model with a horizontal resolution of about 50 km for the atmosphere and 25 km for the ocean. The present climate simulation shows a fairly realistic global TC frequency, seasonal cycle, and geographical distribution. The model has some notable biases in regional TC activity, including simulating too few TCs in the North Atlantic. The regional biases in TC activity are associated with simulation biases in the large-scale environment such as sea surface temperature, vertical wind shear, and vertical velocity. Despite these biases, the model simulates the large-scale variations of TC activity induced by El Niño–Southern Oscillation fairly realistically. The response of TC activity in the model to global warming is investigated by comparing the present climate with a CO_2 doubling experiment. Globally, TC frequency decreases (−19%) while the intensity increases (+2.7%) in response to CO_2 doubling, consistent with previous studies. The average TC lifetime decreases by −4.6%, while the TC size and rainfall increase by about 3% and 12%, respectively. These changes are generally reproduced across the different basins in terms of the sign of the change, although the percent changes vary from basin to basin and within individual basins. For the Atlantic basin, although there is an overall reduction in frequency from CO_2 doubling, the warmed climate exhibits increased interannual hurricane frequency variability so that the simulated Atlantic TC activity is enhanced more during unusually warm years in the CO_2-warmed climate relative to that in unusually warm years in the control climate.

1. Introduction

Tropical cyclones (TCs) are very destructive storms that can cause severe damage due to high winds, rainfall, and storm surge (Pielke et al. 2008; Mendelsohn et al. 2012). Every year, humans suffer serious social and economic damage from TC-induced winds and flooding. Thus, understanding of TC behavior in the context of global climate change is an important issue from both a scientific and socioeconomic perspective.

There have been a number of previous studies simulating TCs using global climate models in order to examine changes in TC frequency under global warming scenarios. The earliest such studies used models with coarse resolutions (about 150–300 km), and typically without full ocean coupling (e.g., Broccoli and Manabe 1990; Haarsma et al. 1993;

* Current affiliation: Ocean Science and Technology School, Korea Maritime and Ocean University, Busan, South Korea.

Corresponding author address: Hyeong-Seog Kim, 201 Forrestal Rd., Princeton, NJ 08540.
E-mail: hyeong-seog.kim@noaa.gov

DOI: 10.1175/JCLI-D-13-00475.1

Bengtsson et al. 1996). As computing power has increased, TC simulations have become more realistic, with Zhao et al. (2009) providing an example of the ability of current atmospheric models to reproduce the interannual variability of Atlantic hurricane counts when forced by observed sea surface temperatures (SSTs). A summary of the most recent generation of such TC–climate studies (Knutson et al. 2010) indicates a growing consensus among models of a reduction in global TC frequency in a warmer climate, with a projected decrease of 6%–34% by the end of the twenty-first century. The present study attempts to further build on these results using a new state-of-the-art high-resolution coupled climate model.

Concerning TC intensity, global climate model simulations of TCs typically have not been able to simulate storms as intense as observed owing to their coarse resolution. However, recent global model studies are progressing toward higher resolution (20–50 km) and more realistic intensity distributions (e.g., Bengtsson et al. 2007; Murakami et al. 2012), albeit without ocean coupling. As a different approach, one way to address the limited resolution of global models has been to use regional dynamical or statistical–dynamical downscaling techniques (Knutson et al. 1998; Emanuel et al. 2008; Bender et al. 2010; Mendelsohn et al. 2012; Knutson et al. 2013). These downscaling techniques use large-scale input from the global models and can provide more realistic distributions of TC intensities. Climate change experiments with these downscaling models, as well as the global model study of Murakami et al. (2012), suggest that the number of TCs that reach category 4–5 intensity (sustained wind speed $>58\,\mathrm{m\,s^{-1}}$) could increase in the future. A recent assessment of TC intensity projection studies finds a 2%–11% increase in response to projected twenty-first century warming (Knutson et al. 2010).

In this study, we analyze global TC activity and its response to climate warming as simulated by the Geophysical Fluid Dynamics Laboratory (GFDL) Climate Model, version 2.5 (CM2.5) (Delworth et al. 2012). The CM2.5 is a coupled atmosphere–ocean–land–cryosphere model that differs from atmospheric GCMs running with prescribed SST by simulating the ocean–atmosphere interaction that is a crucial factor in TC development and intensity. In comparison to other recent efforts using fully coupled models (Gualdi et al. 2008), CM2.5 uses a higher-resolution atmosphere (~50-km grid) and is one of the highest-resolution fully coupled GCMs in use today for such climate change studies.

The rest of this paper is organized as follows. The data for observed TCs and atmospheric and oceanic environments are introduced in the section 2. The model experiments using GFDL CM2.5 are also briefly described in this section. Comparisons between observed and model-simulated climatological TC activity are presented in section 3, and the simulated response to the CO_2 doubling is examined in section 4. Section 5 contains a discussion and conclusions.

2. Data and methods

a. GFDL CM2.5

GFDL CM2.5 is a newly developed high-resolution global climate model, with coupled atmosphere, ocean, land, and sea ice components (Delworth et al. 2012). The model is derived closely from GFDL Climate Model, version 2.1. (CM2.1; Delworth et al. 2006), which was also a fully coupled model and one of the global models used in the Intergovernmental Panel on Climate Change (IPCC) Fourth Assessment Report (AR4). The atmospheric component of CM2.5 uses a finite-volume dynamical core formulated on a cubed-sphere grid (Lin 2004; Putman and Lin 2007) that allows roughly equal-area grid boxes over the globe. The atmospheric model has a horizontal grid spacing of approximately 50 km and a vertical resolution of 32 levels up to 10 hPa. This model uses the relaxed Arakawa–Schubert convection scheme (Moorthi and Suarez 1992) for both deep and shallow convection and the *K*-profile convective boundary layer scheme (Lock et al. 2000). Detailed parameterizations of atmospheric physics are described in Anderson et al. (2004). The ocean component is based on the Modular Ocean Model, version 4.1 (Griffies 2010), and has a horizontal grid spacing of roughly 25 km (from 28 km at the equator to 8–11 km at high latitudes) with 50 vertical levels. For the land and sea ice components, the GFDL Land Model, version 3 (LM3), and Sea Ice Simulator are used, respectively. The simulated climate in CM2.5 showed significant improvement over the tropics compared to CM2.1, including a reduction in biases in the seasonal variation of the intertropical convergence zone (ITCZ) as well as an improved simulation of some aspects of El Niño–Southern Oscillation (ENSO) and its teleconnections (Delworth et al. 2012). In addition, CM2.5 simulates a relatively realistic regional rainfall over the Amazon, Sahel, and Indian monsoon regions and climate over the tropical North Atlantic (Delworth et al. 2012; Doi et al. 2012).

In this study, we use two CM2.5 experiments:

- Control: Present climate experiment—A 280-yr simulation with constant 1990 levels of atmospheric compositions (greenhouse gas and aerosol) and solar irradiance.
- $2 \times CO_2$: CO_2 doubling experiment—A 140-yr simulation, spun off from year 101 of the control simulation, but with a $1\%\,\mathrm{yr^{-1}}$ increase in atmospheric CO_2

concentration for years 1–70 (until CO_2 reaches twice its initial value) and then constant (2 ×) CO_2 concentration for years 71–140.

These experiments are identical to those used in Delworth et al. (2012) and Doi et al. (2013). The simulated SST in the 2 × CO_2 experiment has shown the response of the quasi-steady state to CO_2 doubling after 91 yr [not shown; see Fig. 1 in Doi et al. (2013)]. We thus conduct an analysis only for years 91–140 to focus on the approximate equilibrium response to CO_2 doubling. The analysis period of the control experiment also selected the same period of the 2 × CO_2 experiment.

The TC detection and tracking algorithm used in this study is same as that described in Zhao et al. (2009). The algorithm selects warm-core vortices that satisfy certain criteria in the 6-hourly model outputs and connects them into individual TC tracks. The criteria used in this study are as follows:

- An 850-hPa relative vorticity maximum must be higher than $3.5 \times 10^{-5}\,s^{-1}$.
- The local minimum of sea level pressure, which must be within 2° of the vorticity maximum, is defined as the storm center.
- The local maximum of temperature averaged between 300 and 500 hPa (warm-core center) must be within 2° of the local minima of sea level pressure and the warm-core temperature must be at least 1 K warmer than the surrounding local mean.
- The initial point of the storm trajectory must be between 40°S and 40°N and the distance between two ''connected'' vortex locations must be less than 400 km in 6 h. The trajectory must last at least three days with the maximum wind speed exceeding $17\,m\,s^{-1}$ (not necessarily consecutive).

The TC maximum wind speed is obtained using the lowest level of the atmospheric model (35 m). This wind speed is about 10% larger than the 10-m wind speed that is used for TC intensity in observed TC datasets (Zhao et al. 2012). Thus, using the wind speed at the lowest model level is roughly equivalent to applying a 10% lower intensity criterion on simulated tropical storms than is applied to observed storms. Walsh et al. (2007) suggest that resolution-dependent criteria for sustained TC wind speeds be used in model simulation analyses to reflect the effect of the coarse horizontal resolutions on the intensity of the modeled storms. The 10% reduction in wind speed criterion we use is in the range recommended by Walsh et al. for a 50-km grid model.

In this study we use a 3-day duration criterion for detecting TCs. Because several recent studies used a 2-day criterion instead of 3 days, we also have checked the sensitivity of TC detection to a 2-day duration criterion. As a result, the number of simulated TCs increases globally ($82.0\,yr^{-1}$ for a 3-day criterion vs $113.7\,yr^{-1}$ for a 2-day criterion), resulting in a high bias in the simulated TC counts compared to observations. However, we find that the simulated TC response to the CO_2 doubling (discussed later) is not significantly changed if a 2-day criterion is applied.

b. Observational data

The observed TC data used in the study were obtained from the International Best Track Archive for Climate Stewardship (IBTrACS) data (v03r02) archived by the National Climatic Data Center (Knapp et al. 2010). In this study, we use 6-hourly locations and the intensity of TCs that reach tropical storm intensity (i.e., sustained surface wind speed $>17\,m\,s^{-1}$). We analyze only TCs observed during a recent 30-yr period (1981–2010) to avoid reliability problems in the occurrence and intensity data for TCs during the period prior to satellite observation. For comparison with the simulated TCs in CM2.5, we use only TCs lasting at least 3 days, as this is a criterion we use to detect TCs in CM2.5. We also use the TC size dataset estimated from the Quick Scatterometer (QuikSCAT) surface wind by Chavas and Emanuel (2010) and mean TC size data observations for the western North Pacific retrieved from aircraft data by Weatherford and Gray (1988) for comparison with the simulated TC sizes.

The National Centers for Environmental Prediction (NCEP)–U.S. Department of Energy (DOE) Atmospheric Model Intercomparison (AMIP)-II Reanalysis (R2; Kanamitsu et al. 2002) and National Oceanic and Atmospheric Administration (NOAA) Extended Reconstructed SST, version 3 (ERSST.v3; Smith et al. 2008) are used to evaluate the model-simulated environments affecting TC activity. The datasets were obtained from the FTP site of the NOAA Climate Diagnostics Center; the horizontal resolutions are 2.5° for R2 and 2° for ERSST.v3. The resolutions of these observational datasets are coarser than the model resolution. Thus, we regrid the model outputs to have same resolution as the observational dataset when the model environmental fields are compared to observations. We do not use the atmospheric reanalysis for any trend analysis here for reasons discussed in Vecchi et al. (2013).

3. Present-day tropical cyclone simulation

a. TC climatology

Figure 1 shows the geographical distribution of TC tracks in observations and the CM2.5 control simulation.

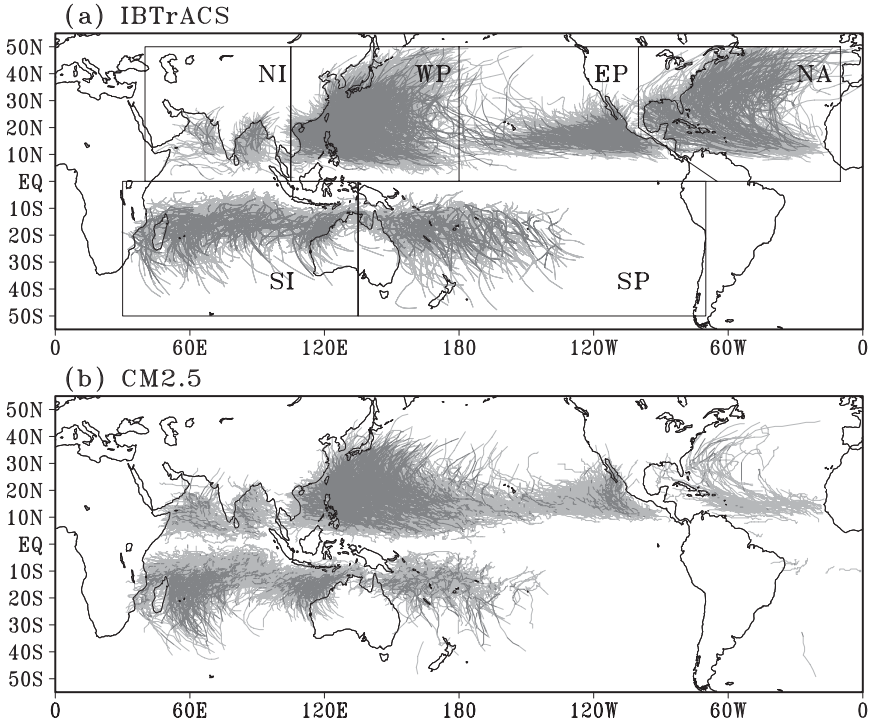

FIG. 1. TC tracks in (a) observations for 1981–2010 and (b) the CM2.5 control simulation for years 110–140. Tropical storm and hurricane intensities are denoted by light and dark gray, respectively.

For comparison of the density of TC tracks in observation and simulation, the simulated TCs are drawn only for years 111–140 (30 yr) in Fig. 1b. For convenience, the global TC activity is divided into seven basins: the North Atlantic (NA), east Pacific (EP), west Pacific (WP), North Indian Ocean (NI), South Indian Ocean (SI), and South Pacific (SP) as denoted in Fig. 1a. The boundaries of the basins are those used in IBTrACS. In observations, TCs form over most of the tropical oceans except for the southeastern Pacific and South Atlantic, which have relatively cool sea surface temperatures and strong vertical wind shear. CM2.5 simulates the general observed geographical characteristics of TC tracks over the globe (Fig. 1b). The observed and simulated annual TC counts in each of the basins are compared in Fig. 2. Although the global TC count simulated in CM2.5 ($82.0\,\mathrm{yr}^{-1}$) shows quite good agreement with observations ($82.4\,\mathrm{yr}^{-1}$), there are substantial biases in TC counts in some basins (Fig. 2). In particular, the number of simulated TCs in the North Atlantic is only about one-quarter of that in observations ($10.7\,\mathrm{yr}^{-1}$ in observations vs $2.7\,\mathrm{yr}^{-1}$ in CM2.5) Several basins have TC counts comparable to the observations ($16.1\,\mathrm{yr}^{-1}$ in observations vs $16.6\,\mathrm{yr}^{-1}$ in CM2.5 for EP, $26.1\,\mathrm{yr}^{-1}$ vs $27.5\,\mathrm{yr}^{-1}$ for WP, and $4.7\,\mathrm{yr}^{-1}$ vs $5.5\,\mathrm{yr}^{-1}$ for NI). Here, it is notable that the EP basin in this study covers the central Pacific region. The TC counts in the central Pacific region (180°–140°W) are $1.4\,\mathrm{yr}^{-1}$ in observations and $5.3\,\mathrm{yr}^{-1}$ in CM2.5 while those in the eastern EP (west of 140°W) are $14.7\,\mathrm{yr}^{-1}$ in observations and $11.3\,\mathrm{yr}^{-1}$ in CM2.5, indicating a positive (negative) bias of TCs in the central (eastern) North Pacific region.

Examining the simulated TCs over the NA in more detail, most of the model TCs located there formed over the vicinity of the main development region (MDR; 10°–20°N, 80°–20°W; Goldenberg and Shapiro 1996); TC formation is especially deficient over the Gulf of Mexico and east of Florida. Meanwhile, in the central North Pacific (170°–150°W) and Arabian Sea (west of 75°E) CM2.5 simulates more TC activity than observed (Chu 2002;

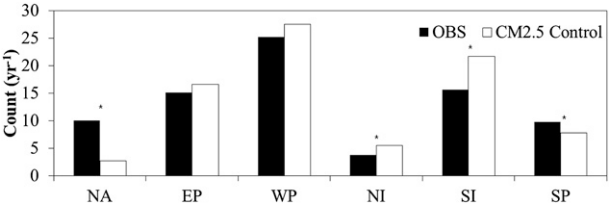

FIG. 2. Observed (1981–2000) and simulated (CM2.5 control run) annual TC counts in each basin (yr^{-1}). A statistically significant difference ($p < 0.01$) with the two-sided Student's t test is denoted by an asterisk (*).

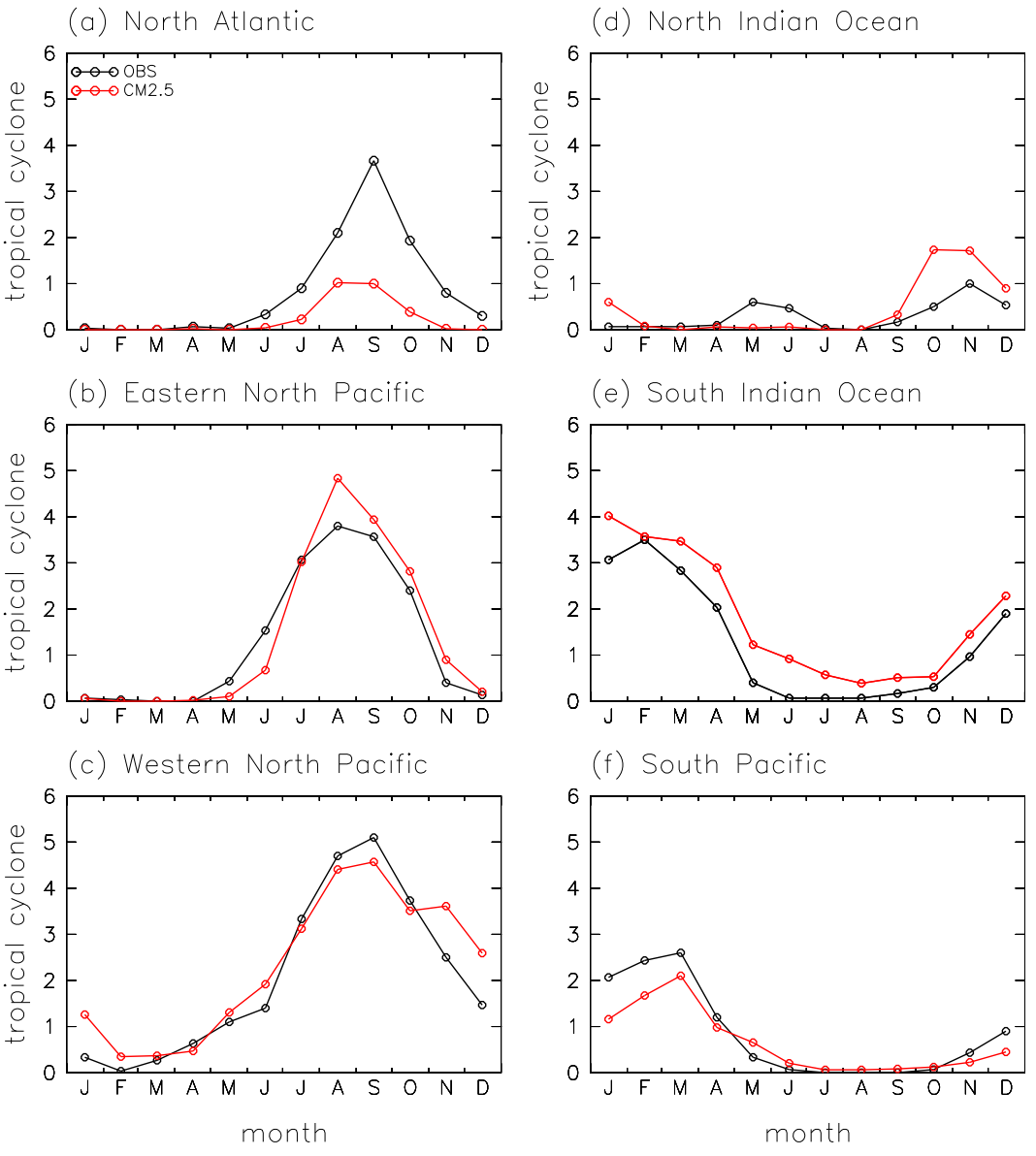

FIG. 3. The annual cycle of monthly TC frequency in observations and the CM2.5 control simulation (yr^{-1}).

Evan and Camargo 2011), contributing to slightly positive biases in the simulated TC activity over the North Pacific and North Indian Ocean as a whole. In the Southern Hemisphere, CM2.5 produces more TCs than observed over the South Indian Ocean (16.0 yr^{-1} in observations vs 21.7 yr^{-1} in CM2.5) and fewer than observed in the South Pacific (10.9 yr^{-1} in observations vs 7.8 yr^{-1} in CM2.5).

As a sensitivity test, we used weaker criteria for TC detection (e.g., 12 m s^{-1} for wind speed, 0.75 K for warm core, and/or 2 days for duration) to see the effect on the TC count in the NA. The results show that even if we applied weaker criteria, a substantial negative bias over the North Atlantic remains. This indicates that the CM2.5 simulation has systematic biases that suppress TC activity in this vicinity, as will be discussed later.

Figure 3 presents the seasonal cycle of observed and simulated TCs in each of the basins. The model shows a fairly realistic seasonal cycle of TC counts, with a peak during the summer season of each hemisphere except for the North Indian Ocean. For the North Indian Ocean, the observed seasonal cycle of TCs has a bimodal shape with peaks in both boreal spring and fall, as the TC activity in this basin is suppressed by strong vertical wind shear during the summer monsoon season. CM2.5 captures only one of these peaks (the postmonsoon season).

Although the number of TCs over the North Atlantic in CM2.5 is smaller than the observation for all months, the phase behavior of the TC season in the North Atlantic is captured fairly well although the simulated seasonal cycle peaks slightly earlier than in observations (Fig. 3a). As noted earlier, the model has positive bias in TC counts in the central North Pacific region (Fig. 1). The model TCs in the central North Pacific region are active during August–October (not shown), affecting the positive bias in the annual peak of the monthly TC counts in the EP basin. For the other basins, the positive bias in the monthly number of TC formation tends to be found in the mid- and late TC seasons rather than early season.

To investigate the environmental factors affecting the aforementioned characteristics of the TC activity in CM2.5, the SST, vertical wind shear, and 500-hPa vertical pressure velocity $\omega_{500\,\mathrm{hPa}}$ are analyzed as potential contributing factors (Fig. 4). The vertical wind shear is computed as the amplitude of the difference vector between winds at 200 and 850 hPa. Figure 4 shows the model bias in these fields during boreal summer (July–October) for the Northern Hemisphere and austral summer (December–March) for the Southern Hemisphere. During the boreal summer, the SST simulated in CM2.5 has a cold bias in the North Atlantic and much of the subtropical western and central North Pacific. The model has a warm bias in the eastern North Pacific and much of the North Indian Ocean (Fig. 4a). Although the SST bias is smaller in CM2.5 than in the lower-resolution CM2.0 and CM2.1, significant biases remain as discussed by Doi et al. (2012). Along with the cold SST bias in the North Atlantic, CM2.5 simulates stronger vertical wind shear over the tropical and subtropical North Atlantic during boreal summer (Fig. 4b). The warm bias in the eastern Pacific and cold bias in the North Atlantic in CM2.5 may lead to a strong vertical wind shear bias and anomalous descent over the NA basin, analogous to ENSO effects on the Atlantic region (Goldenberg and Shapiro 1996; Vecchi and Soden 2007). These model biases would all act to inhibit CM2.5 from producing TCs over the North Atlantic basin. Meanwhile, CM2.5 has a negative bias in the vertical wind shear between 200 and 850 hPa and $\omega_{500\,\mathrm{hPa}}$ (i.e., anomalous rising motion) over the central and eastern tropical North Pacific and the Arabian Sea (Figs. 4a–c), which would be expected to lead to more vigorous TC activity in these regions. For the Southern Hemisphere basins, CM2.5 simulates vertical wind shear that is generally too strong, anomalous sinking motions, and a cold SST bias over the tropics and subtropics in the South Pacific during austral summer (Figs. 4d–f). Although these factors would act to suppress TC activity in the Southern Hemisphere, there does not appear to be an overall bias in TC frequency in the South Pacific and Indian Ocean. It is also notable that, although the number is small, the TCs over the South Atlantic in CM2.5 are formed over the northern edge of the South Atlantic where there is a warm bias of SST in CM2.5 rather than the southeast offshore of Brazil where observed TC Catarina developed in March 2004.

TC activity over the NA basin is known to have a strong statistical relationship with the vertical wind shear over the MDR (e.g., Goldenberg and Shapiro 1996; Landsea et al. 1998; Wang et al. 2009). Figure 5 illustrates the relationship between the vertical wind shear and the Atlantic tropical cyclones during August–October in both observations and CM2.5. The MDR vertical wind shear and Atlantic TC counts are negatively correlated in observations ($r = -0.60$) as well as the CM2.5 control ($r = -0.41$). The MDR vertical wind shear values in CM2.5 simulations are much higher than those in the observations (Fig. 5). The Atlantic TC activity would apparently be suppressed even in observations if the magnitude of the vertical wind shear were as strong as in CM2.5. Interestingly, the overall bias in shear and NA TC frequency in this model is consistent with an extrapolation of the observed shear–TC relationship.

In summary, we conclude that the bias of simulated TCs, including significant negative bias of TCs in the NA basin, is likely largely a response of CM2.5 to biases in its simulated large-scale climatology. This further suggests that the simulation skill for TC activity in the model could be improved if the model biases in climatological environments such as SST and wind shear were reduced.

b. *ENSO-related variation*

The variation of TC activity is related to large-scale environments such as ENSO, the North Atlantic Oscillation, the Atlantic multidecadal oscillation, and monsoons. To explore the simulation of the variation of TC activity related to large-scale environments in CM2.5, we focus on the relationship between the model's TC activity and ENSO, since ENSO is known to be a key phenomenon affecting the interannual variation of TC activity over the global tropics (e.g., Nicholls 1979; Wang and Chan 2002; Camargo and Sobel 2005; Kuleshov et al. 2008; Klotzbach 2011). It is noted that CM2.5 has a marked improvement in the simulation of ENSO (but still has some bias vs the observations) and its related large-scale circulation anomalies compared to earlier GFDL models such as CM2.1 [see Figs. 17–19 in Delworth et al. (2012)]. Figure 6 shows a map of TC occurrences regressed on the seasonal mean Niño-3.4 index (average of SST anomaly over the region 5°N–5°S, 170°–120°W). Here, the TC occurrence is defined as the number of TC days accumulated over the summer season: June–October for the Northern Hemisphere

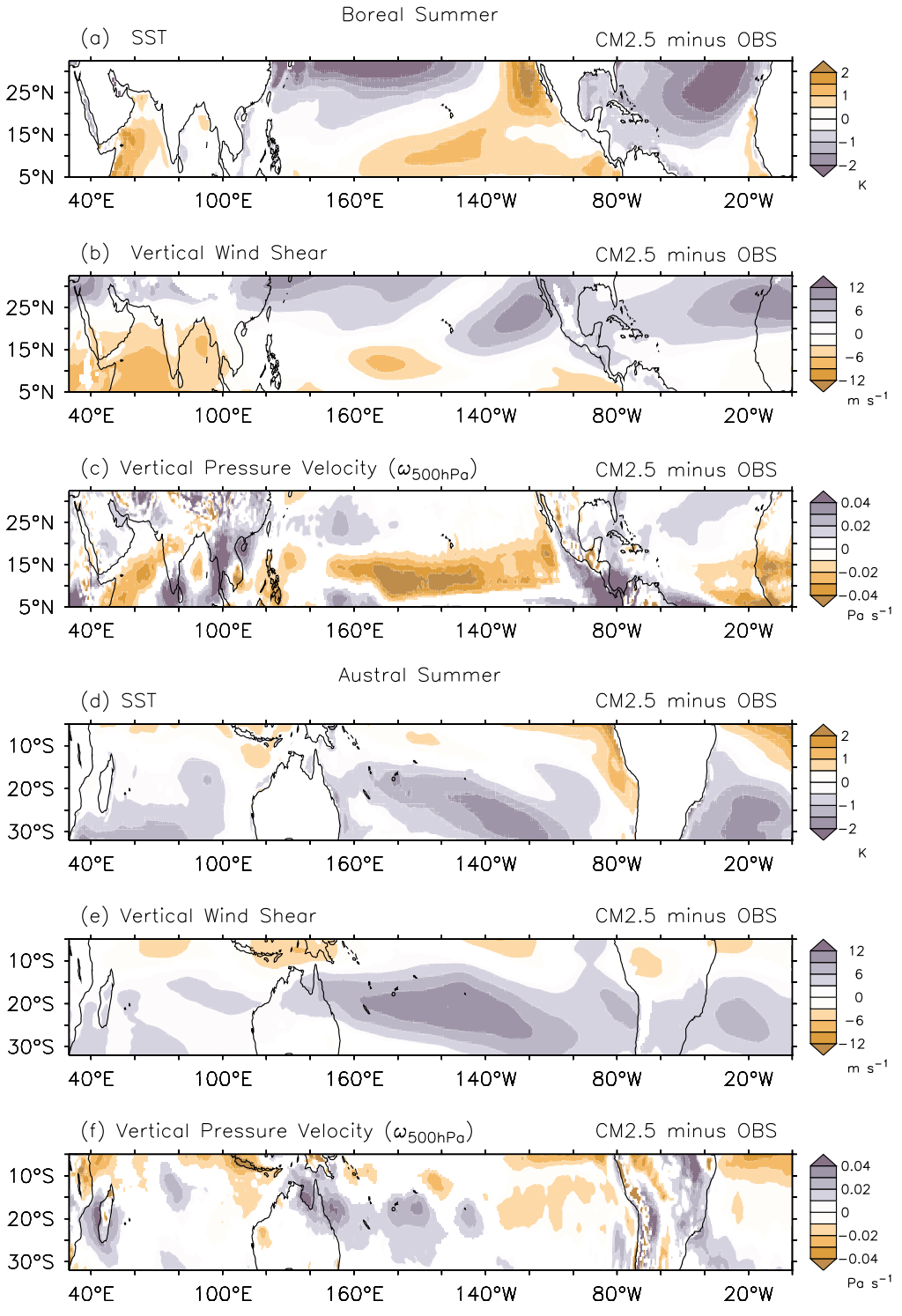

FIG. 4. Bias in the CM2.5-simulated (a),(d) SST (K); (b),(e) vertical wind shear between 200 and 850 hPa ($m\,s^{-1}$); and (c),(f) $\omega_{500\,hPa}$ ($Pa\,s^{-1}$) compared to observations for (top) boreal and (bottom) austral summer. Warm (cold) colors represent environments that are generally more (less) favorable for TC development in CM2.5 compared with observations. Only statistically significant regions ($p < 0.05$) using a two-sided Student's *t* test are shaded.

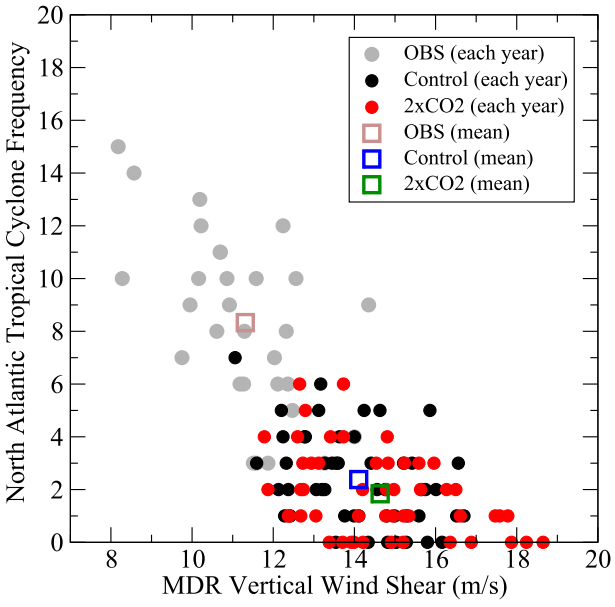

FIG. 5. Scatterplot of the vertical wind shear over the MDR vs the number of TCs over the Atlantic basin during August–October. Observations (gray dots) are based on the IBTrACS and R2 datasets for 1981–2010. CM2.5 simulation results are shown in black (control run) and red ($2 \times CO_2$ run). The mean value of each of the samples is marked by an open square. Unit for frequency is yr^{-1}.

(Figs. 6a,b) and December–March for the Southern Hemisphere (Figs. 6c,d). We used 6-hourly TC track information obtained from the IBTrACS and the CM2.5 simulation. These simultaneous (unlagged) regression results for the Niño-3.4 index reproduce well-known ENSO-dependent TC variations in both hemispheres (Figs. 6a,c). Because there are biases in both TC activity (Fig. 1) and the amplitude and frequency of ENSO (Delworth et al. 2012), we focus on the qualitative relationship between the ENSO and TC activity using the regression analysis rather than the quantitative relationship. During El Niño, the boreal summer TC activity increases in the southeastern part of the western North Pacific and central/eastern North Pacific, and decreases in the northwestern part of the western North Pacific and North Atlantic, with opposite changes during La Niña. For the Southern Hemisphere, enhanced TC activity is observed during El Niño over the South Pacific while TC activity is reduced in the regions off the northwestern coast of Australia, again with opposite changes during La Niña (Fig. 6c). As shown in Figs. 6b and 6d, the CM2.5 simulations show good agreement with key features of the observed ENSO signal in TC activity, such as the eastward shift of TCs in the western North Pacific (Fig. 6b) and enhancement of TC activity in the South Pacific (Fig. 6d), although the actual quantity of the TC variability regressed on the ENSO index does not quantitatively match that in the observations (e.g., the ENSO-related decrease in the TC activity is too small in the extreme western North Pacific and too large in the eastern North Pacific). A weak negative statistical relationship between El Niño and North Atlantic TC activity is also seen in CM2.5 (Fig. 6). However, the correlations are significant for only for a few grid boxes for observations or the model, and these regions are not in the same parts of the basin for model and observations. The results show that CM2.5 has skill to simulate much of the geographic structure of the relation between the TC activity and ENSO. The variation of TC activity in relation to ENSO in the observations has been attributed to changes in the vertical wind shear and relative vorticity forced by the zonal gradient of tropical SST anomalies associated with ENSO (Wang and Chan 2002; Camargo et al. 2007). The improved ENSO simulation characteristics in CM2.5 (Delworth et al. 2012) likely help with the successful simulation of ENSO-related TC activity changes. Overall, our analysis suggests that CM2.5 has sufficient realism to be useful for exploring the TC response to the changes in the large-scale environments, such as could occur with greenhouse gas–induced climate warming.

4. Changes in TC activity in response to CO_2 doubling

The response of TC activity in CM2.5 to a CO_2 doubling is investigated in this section. The basic statistics for changes in TC activity in response to CO_2 doubling are given in Tables 1 and 2. Table 1 shows the annual number of TCs that reach tropical storm ($17\ m\ s^{-1}$) and hurricane ($33\ m\ s^{-1}$) surface wind speed intensity levels in the control run and the changes in response to CO_2 doubling in CM2.5 simulation. In Table 2, the percentage changes in TC-related parameters such as maximum wind speed, lifetime, travel distance, translation speed, and power dissipation index (PDI) in response to CO_2 doubling are shown. In these tables, statistically significant changes are marked with an asterisk ($p < 0.01$) or open circle ($p < 0.05$)[1] on the basis of a two-sided t test.

a. Frequency

As shown in Table 1, CM2.5 simulates a significant reduction of TC genesis in response to CO_2 doubling, which is consistent with a number of previous studies (e.g., Knutson et al. 2010). A significant reduction is

[1] The p value represents the level of significance at which the null hypothesis would be rejected: for example, $p < 0.01$ (0.05) denotes the statistically significance at the 99% (95%) confidence level.

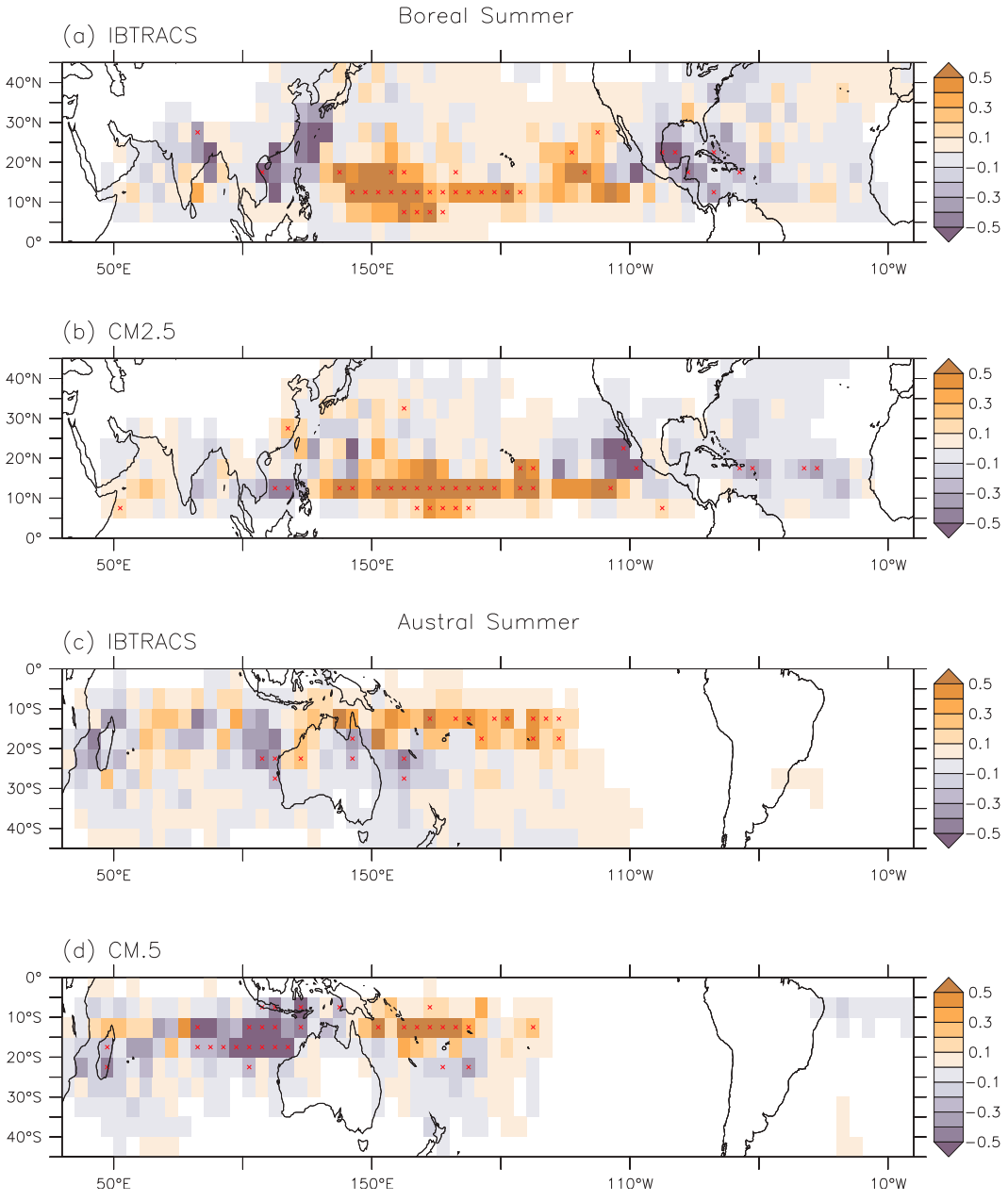

FIG. 6. TC occurrences (day yr^{-1}) for each 5° × 5° grid box regressed on the Niño-3.4 index in (a),(c) observations and (b),(d) the CM2.5 simulation for (top) boreal and (bottom) austral summer. Statistically significant regions ($p < 0.05$) using a two-sided Student's t test are marked with a red cross.

simulated in each of the six individual basins (Table 1). The magnitudes of these changes (−19% for the globe with values ranging from −13% in the North Indian Ocean to −30% in the North Atlantic) are in general agreement with values from previous studies (Yoshimura et al. 2006; Bengtsson et al. 2007; Knutson et al. 2010; Murakami et al. 2011; Held and Zhao 2011), yet most of these studies showed regions of increase and decrease in contrast with the ubiquitous decrease seen here. The global number of TCs developing to hurricane strength (maximum wind speed >33 m s^{-1}) also decreases significantly ($p < 0.05$) (−9.2%) using the two-sided t test. The fractional decrease, however, is smaller than for all TCs and a consistent signal is not seen across all basins, with only the South Indian Ocean decrease being significant. The fraction of TCs that reaches hurricane intensity increases in most basins with the largest increases simulated in the Northern Hemisphere basins. These results

TABLE 1. Changes in the annual number of TCs that reach tropical storm and hurricane intensity thresholds in response to a CO_2 doubling in CM2.5. Statistically significant changes are denoted by an asterisk (*) for $p < 0.01$ and open circle (°) for $p < 0.05$ using the two-sided Student's t test.

	Tropical storms (A)			Hurricanes (B)			Ratio [100(B/A)]	
	Control (yr^{-1})	$2 \times CO_2$ (yr^{-1})	Change (%)	Control (yr^{-1})	$2 \times CO_2$ (yr^{-1})	Change (%)	Control (%)	$2 \times CO_2$ (%)
Global	82.0	66.6	−18.8*	31.6	28.7	−9.2°	38.5	43.1*
NA	2.7	1.9	−29.6*	0.4	0.3	−25.0	14.8	15.8
EP	16.6	13.9	−16.3*	3.0	3.5	16.7	18.1	25.2*
WP	27.5	23.1	−16.0*	14.4	13.3	−7.6	52.4	57.6°
NI	5.5	4.8	−12.7°	2.0	2.0	0.0	36.4	41.7°
SI	21.7	16.5	−24.0*	8.8	6.8	−22.7*	40.6	41.2
SP	7.8	6.3	−19.2°	3.1	2.6	−16.1	39.7	41.3

indicate that the model-simulated TCs are intensified in the $2 \times CO_2$ climate, although their frequency is reduced, which is consistent with previous studies (e.g., Knutson et al. 2010).

b. *Intensity, lifetime, travel distance, and translation speed*

Figure 7 shows box-and-whisker plots that illustrate statistical distributions of the lifetime-maximum wind speeds and lifetimes of TCs simulated in CM2.5 control and $2 \times CO_2$ experiments. In terms of global statistics, the maximum wind speed increases systematically in the $2 \times CO_2$ simulation for all percentiles examined (i.e., 1st, 25th, 50th, 75th, and 99th percentiles). It is noted that this model cannot simulate very intense TCs [e.g., none is simulated with the lowest model level wind speed exceeding $50\,m\,s^{-1}$, which is the Saffir–Simpson surface wind speed threshold for major hurricanes (categories 3–5)]. This is a qualitatively similar limitation of TC simulations to that using other dynamical models with similar horizontal resolutions (e.g., Zhao et al. 2009). The percent change in the mean of the global TC maximum wind speed distribution is 2.7%. The difference between the two global distributions in Fig. 7 is statistically significant ($p < 0.01$) using a two-sided Mann–Whitney–Wilcoxon (MWW) test. The MWW test is a nonparametric test that examines the ranks of all elements in the two target sets. It is more suitable for testing the box-and-whisker plots that show the distribution of the elements in the sample sets. This test is robust to the outliers and does not require the sample sets to be normally distributed. The increase in mean TC maximum wind speed is statistically significant in the Northern Hemisphere basins (2.5%–4.6%) while it is smaller and not significant in the Southern Hemisphere basins (1.5%–2.0%) (Fig. 7, Table 2). It is also notable that the box-and-whisker plots show a larger increase in the highest percentile of TC wind speed than the percentiles including the median, suggesting an enhanced climate change signal for the stronger storms, reminiscent of that found in some observational studies of intensity (e.g., Elsner et al. 2008). Despite the model's limitation in simulating intense TCs, we can cautiously infer an increase in stronger TCs in the CO_2-warmed climate from our results. Our global TC intensity change results seem generally consistent with projections from other recent studies using dynamical downscaling methods, although those also used different future climate forcing scenarios. For example, Bender et al. (2010) and Knutson et al. (2013) show a fairly robust enhancement in the frequency of very intense TCs in category 4–5 in their model future, although this change was smaller for the representative concentration pathway 4.5 (RCP4.5) multimodel projections of phase 5 of the Coupled Model Intercomparison Project (CMIP5) than for the CMIP3 A1B emissions scenarios. It is worth noting that the CMIP5 RCP forcing scenario sources include changes to climate forcing agents other than

TABLE 2. Changes in mean TC-related parameters (%): lifetime-max wind speed, lifetime, track distance, translation speed, PDI per TC; and annually accumulated PDI. Statistically significant changes are denoted by an asterisk (*) for $p < 0.01$ and open circle (°) for $p < 0.05$ using the two-sided Student's t test.

	Global	NA	EP	WP	NI	SP	SI
Max wind speed (%)	2.7*	4.3°	4.6*	2.5*	3.2°	2.0	1.5
Lifetime (%)	−4.6*	−2.0	−0.6	−5.8*	−3.6	−4.4	−7.8*
Travel distance (%)	−4.0*	−1.7	0.6	−5.0°	−1.8	−4.0	−10.5*
Translation speed (%)	0.6	2.7	0.9	1.7	6.9°	−0.8	−3.0°
PDI (%)	3.4°	12.7	12.0*	3.1	5.0	2.3	−3.8
Annually accumulated PDI (%)	−3.5	−10.6	−7.1	−4.6	3.4	−7.6	−11.9°

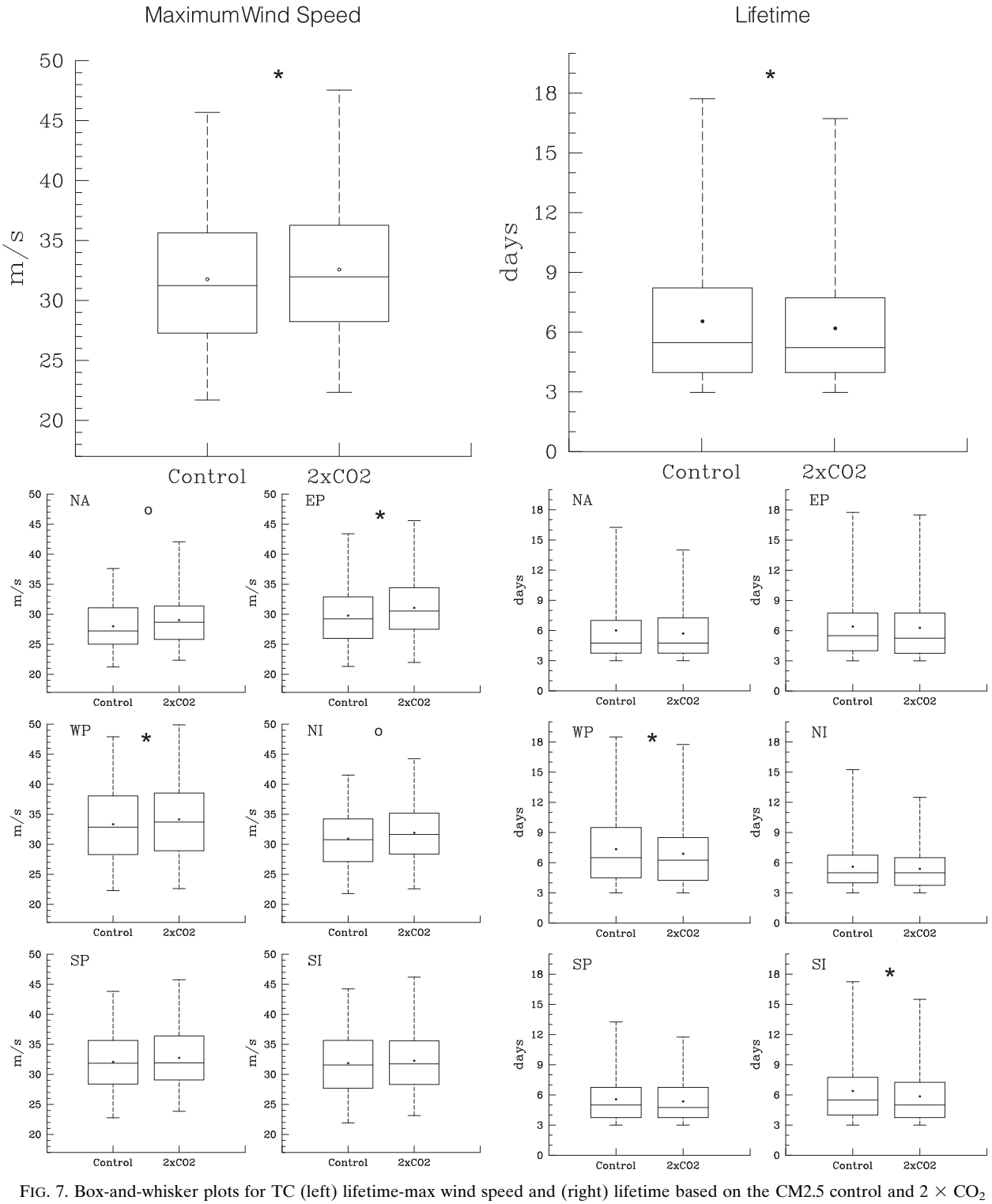

FIG. 7. Box-and-whisker plots for TC (left) lifetime-max wind speed and (right) lifetime based on the CM2.5 control and 2 × CO_2 experiments. The two plots at (top) are for global TCs while the other plots at (bottom) are for the individual basins. The boxes denote the lower and upper quartiles (25th and 75th percentiles), and the band near the middle of the box is the median of the samples. The whiskers extend to the 1st and 99th percentiles and the dot indicates the mean of each sample. The significance of differences between the control and 2 × CO_2 sample means for each basin or the globe is assessed using the two-sided MWW test. Significant differences are denoted by the asterisks (*) for $p < 0.01$ and open circles (°) for $p < 0.05$.

greenhouse gases, whereas the present study focuses solely on the influence of CO_2 changes.

The simulated TC lifetimes (Fig. 7, Table 2) become shorter on average in the $2 \times CO_2$ simulation. The TC lifetime is defined as the duration calculated by the TC detection algorithm used in this study. Because of the criterion for TC duration in the TC detection algorithm, there is little change in the lowest bounds for lifetime. The changes, however, become larger at the upper percentiles. The change in the global TC lifetime distribution is statistically significant ($p < 0.01$), with a change in the mean of −4.6%. Similar reductions are also found over most of the individual basins although the significant changes are found only in the western North Pacific and South Indian Ocean (Fig. 7, Table 2). It is noted that this decrease in the TC lifetimes is not consistent with the results of Bengtsson et al. (2007), who found a minor increase in the lifetimes of TCs in their climate warming experiments.

We also have examined the TC travel distance (track length) and found that this decreases globally. The percent changes in each of the individual basins tend to mirror the changes in TC lifetime (Table 2) in terms of magnitude and statistical significance. The translation speed of TCs shows no significant changes globally between the control and $2 \times CO_2$ experiments, which is consistent with the results of a recent downscaling study for the Atlantic basin only, using CMIP5 (Knutson et al. 2013). The translation speed of TCs is one of the major factors influencing the potential damage from TCs because slow-moving TCs have a greater possibility to afflict a larger area with a longer duration of strong winds (Mahendran 1998; Holland et al. 2010). Our results suggest that the contribution of translation speed changes to potential damage changes from TCs may be minor in this type of greenhouse gas–induced warming scenario.

c. TC size

The TC size is also recognized as an important parameter influencing TC damage potential because it roughly controls the width of the ''damage swath'' induced by strong wind gusts of landfalling TCs (Powell and Reinhold 2007; Maclay et al. 2008) and can also contribute to the magnitude and areal extent of the storm surge, as illustrated by U.S. Hurricanes Isabel (2003), Katrina (2005), and Sandy (2012). In this study, we examine TC sizes using a mean radius of 12 (R12), 15 (R15), and 25 m s^{-1} (R25) azimuthally averaged tangential wind speeds. This wind speed metric is used in our calculation of TC size to reduce the influence of the background wind. Figure 8 shows the mean TC size for each basin in the control and $2 \times CO_2$ experiments. Overall, the control run–simulated TC sizes are systematically larger than those estimated from observations, except in the NA where the simulated TCs are smaller. This could be due to the horizontal grid spacing (~50 km) of CM2.5 limiting the model's ability to simulate small TCs. In terms of the interbasin differences in TC sizes, CM2.5 correctly simulates the largest TCs over the western North Pacific, but the dramatically smaller average TCs over the eastern North Pacific in observations is a feature not well captured in the model, indicating further room for improvement, perhaps in future models with higher resolution. In response to CO_2 doubling, the mean simulated TC size, as measured by R12 and R15, increases significantly, according to a two-sided t test, both over the globe and in each of the individual basins except for the South Indian Ocean. The changes in global mean TC size for R12, R15, and R25 are 3.3%, 2.4%, and 4.4%, respectively, with similar

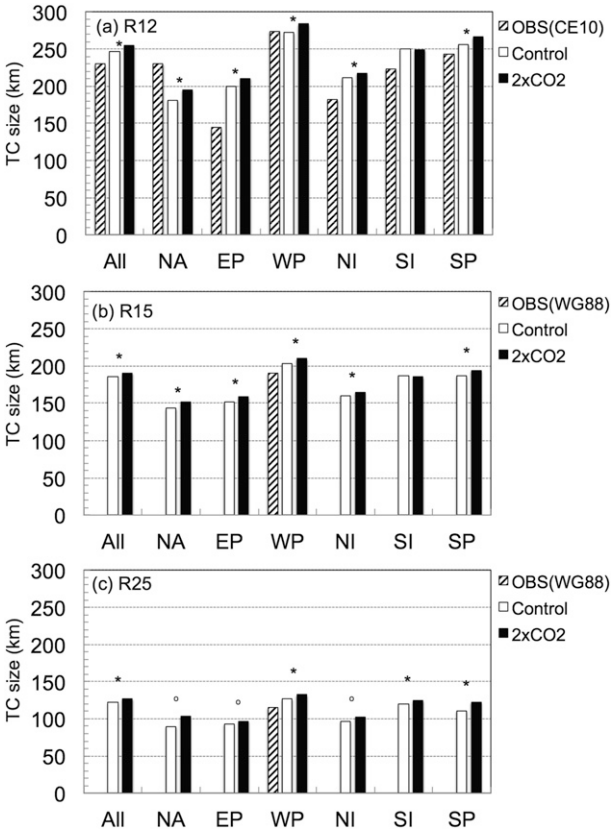

FIG. 8. Mean TC size, defined as the radius of (a) 12 (R12), (b) 15 (R15), and (c) 25 m s^{-1} (R25) azimuthally averaged tangential winds in the control (open bar) and $2 \times CO_2$ (filled bar) simulations for each basin. The observational climatology of R12 (Chavas and Emanuel 2010) for all basins and R15 and R25 (Weatherford and Gray 1988) for the northwest Pacific (WP) basin are plotted as dashed bars. Significant differences between the mean TC sizes in the control and $2 \times CO_2$ experiments are denoted by asterisks (*) for $p < 0.01$ and open circles (°) for $p < 0.05$ based on the two-sided Student's t tests.

increases being found over most of the basins. Although there is a negative bias in TC size in the control run over the North Atlantic, the increase in TC size in the 2 × CO_2 experiment is statistically significant. The South Indian Ocean has a significant TC size increase, but only for the R25 metric.

The results indicate that the coverage of strong TC wind gust may become larger in a warmed climate. The TC size is influenced by TC intensity as well as TC location, formation mechanism, and surrounding environments. Because the definition of TC size in this study is based on TC wind speed, we speculate that the increase in TC intensity might be a main factor causing the TC size increase in response to CO_2 doubling. However, further study is needed to explore the possible influence of other factors.

d. TC rainfall

Heavy rainfall induced by TCs is another important source of TC damage, and is projected to increase with climate warming (Knutson et al. 2010, 2013). We examine the CO_2-induced changes in the TC rainfall in the CM2.5 simulations. Figure 9 shows the fractional changes, between the control and 2 × CO_2 simulations, of average TC-related rainfall rates within 150, 250, 350, and 450 km of the TC center, using all the TC periods in these experiments. The results show a significant increase in rainfall rate near TCs in response to CO_2 doubling (significance assessed using a two-sided t test, $p < 0.05$). The fractional increase in rainfall rate near the storms is much higher than the fractional increase in climatological rainfall over tropical oceans in general (+3.8% averaged over 30°S–30°N). The global mean changes of TC rainfall rates are 12.2%, 13.3%, 12.1%, and 11.3%, for averaging radii of 150, 250, 350, and 450 km, respectively, but the rates vary from basin to basin. The fractional change near the storm features a maximum increase for a 250-km averaging radius from the TC center, and smaller increases at larger (e.g., 350 or 450 km) or smaller (150 km) averaging radii. Knutson et al. (2013) found that the fractional increase in TC rainfall becomes larger for smaller averaging radii; in their experiments, this increase continued down to an averaging radius of 50 km [see Fig. 11 in Knutson et al. (2013)]. The discrepancy between the Knutson et al. (2013) results and the CM2.5 results in Fig. 9 may result from the coarser model resolution used in our experiments [i.e., models with 18- and 9-km grids were used in Knutson et al. (2013) vs about 50 km for CM2.5].

If we assume that the moisture convergence from the larger-scale environments dominates the moisture budget near the TC, the mean increase in TC rainfall rate follows roughly the changes expected based on

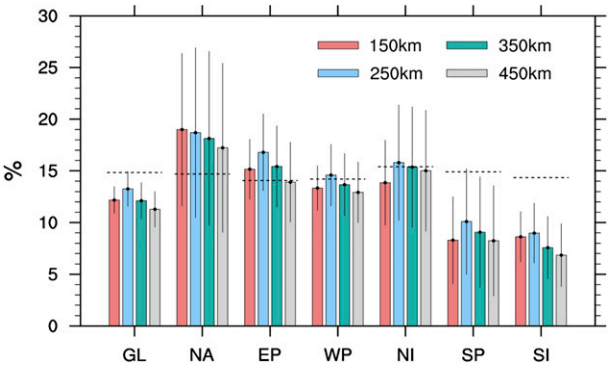

FIG. 9. The fractional change of rainfall rate averaged within 150, 250, 350, and 450 km of the TC center for the globe and each basin in response to CO_2 doubling. The error bars denote 95% confidence intervals. Two-sided Student's t tests indicate that all of the [(2 × CO_2) − control] differences are statistically significant ($p < 0.05$). The dotted lines represent the approximate changes of the water holding capacity for each basin (estimated as 7% °C^{-1} increase of basin-averaged SST).

increases in the environmental water holding capacity of the atmosphere (which increases at about 7% 1°C^{-1} SST warming; see also Knutson et al. 2013). Based on an increase in tropical SST of about 2.1°C in the CM2.5 CO_2 doubling experiment, the fractional increase in the environmental low-level water vapor content is about 14.7%. The water vapor content increases for each individual basin are similar (dotted bars in Fig. 9). While the percent increases of the estimated lower tropospheric water vapor content for the Northern Hemisphere basins are similar to the simulated fractional changes of TC rainfall, the simulated TC rainfall response in the Southern Hemisphere basins is much smaller (Fig. 9). This result is reminiscent of the TC intensity response in the model, in which the increase in TC intensity in the Southern Hemisphere basins was smaller than in the Northern Hemisphere (Table 2). The result suggests that TC intensity changes may play an important role (along with environmental water vapor changes) in the response of TC rainfall rates to large-scale climate warming.

e. Global distribution of TC response to CO_2 doubling

Figure 10 shows maps of raw differences and percentage changes in the TC occurrence, maximum wind speeds, and the annually accumulated PDI for each 5° × 5° grid box, comparing the CM2.5 control and 2 × CO_2 simulations. A 9-point Gaussian smoothing filter was applied to the maps for display purposes, and statistically significant changes at the regional scale are indicated by the red contours in Fig. 10 (right). The PDI as defined by Emanuel (2005) is the integral of the cube of

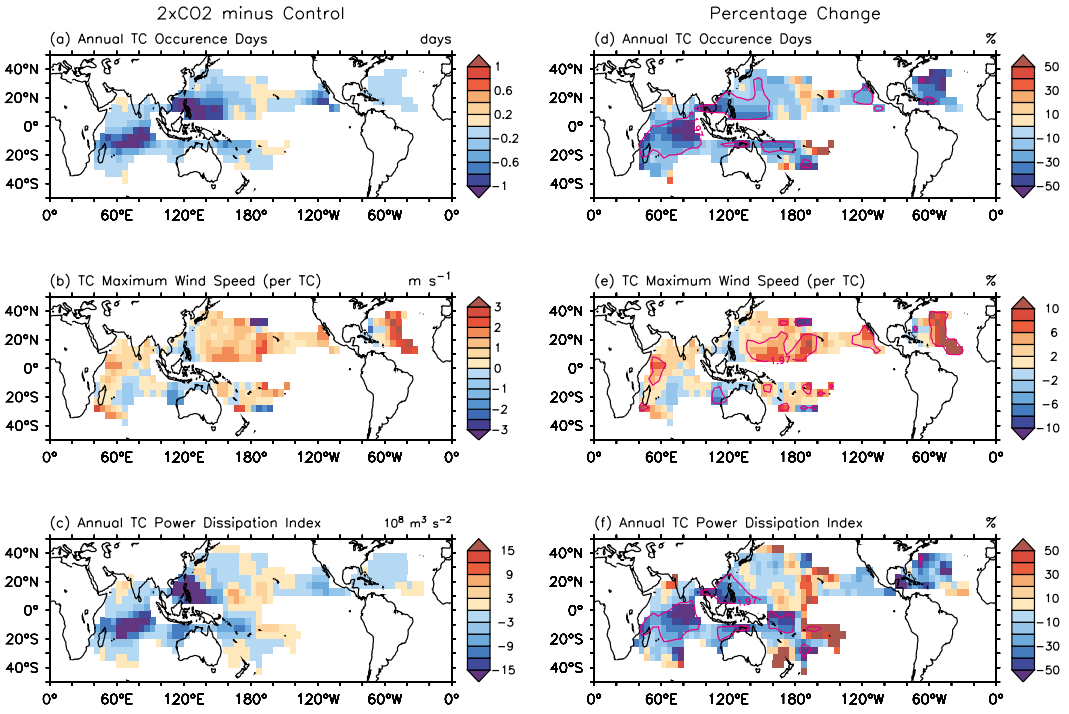

FIG. 10. Differences and percentage change between the CM2.5 control and 2 × CO_2 simulations in the (a),(d) annual TC occurrence days; (b),(e) lowest model level wind speed averaged across all TC occurrences; and (c),(f) annual accumulated PDI in each 5° × 5° grid box. A Gaussian smoothing filter was applied to the gridded values before plotting. Red contours (right) denote statistical significance at the $p < 0.05$ level using the two-sided Student's t test.

each TC's maximum wind speed, integrated over the TC lifetime and over each TC occurring during the year. PDI is related to the overall power dissipation (Emanuel 2005), which represents the total energy dissipated by the tropical storm over its lifetime and integrates over a storm's entire surface wind field. In the figure, the PDI is accumulated over each TC's occurrence time in each grid and over the entire year, and thus represents an annual measure of the potential destructiveness of TCs (Emanuel 2005). By definition, the PDI is amplified to the power of 3 as the wind speeds of TCs increase. Thus, the PDI may be significantly biased low in CM2.5 since the model cannot simulate very intense TCs (e.g., Fig. 7).

Consistent with the reductions in the TC formation and lifetimes in the warm climate, a substantial decrease is seen in the TC occurrence days over the global tropics and subtropics (Figs. 10a,d). The largest absolute decreases are simulated over the western North Pacific, extreme eastern North Pacific, and South Indian Ocean. This change is similar to the results of Zhao and Held (2012) and Murakami et al. (2012) that showed decreases of TC occurrence in the western part of the western North Pacific and an increase in the central Pacific in a warm-climate simulation (although using a different forcing scenario than the 2 × CO_2 perturbation that we use). The percentage reduction of TC occurrence is most pronounced in the Atlantic and Indian Oceans and over the westernmost parts of the North and South Pacific basins. The regional changes are statistically significant mainly over the Indian Ocean and much of the western and northeast Pacific basins.

The average sustained TC wind speed increases over most tropical storm regions except for the eastern part of the South Indian Ocean (Figs. 10b,e). The percentage increase in TC wind speeds is most pronounced and statistically significant over a swath of the central Atlantic basin, large parts of the three Pacific storm basins, and along the western edge of the Indian Ocean basin. The change is not statistically significant in the immediate vicinity of some key TC landfalling regions, including the Philippines, much of Southeast Asia, and the eastern Gulf of Mexico/Florida/Caribbean region. A significant reduction is simulated in a small region near northwestern Australia.

Although the TC occurrence and intensity have generally opposite directions of changes, the regional pattern of changes in PDI (Figs. 10c,f) tends to be more similar to those for TC occurrence than for intensity. The opposing changes in the accumulated PDI versus TC intensity might occur because the changes in TC

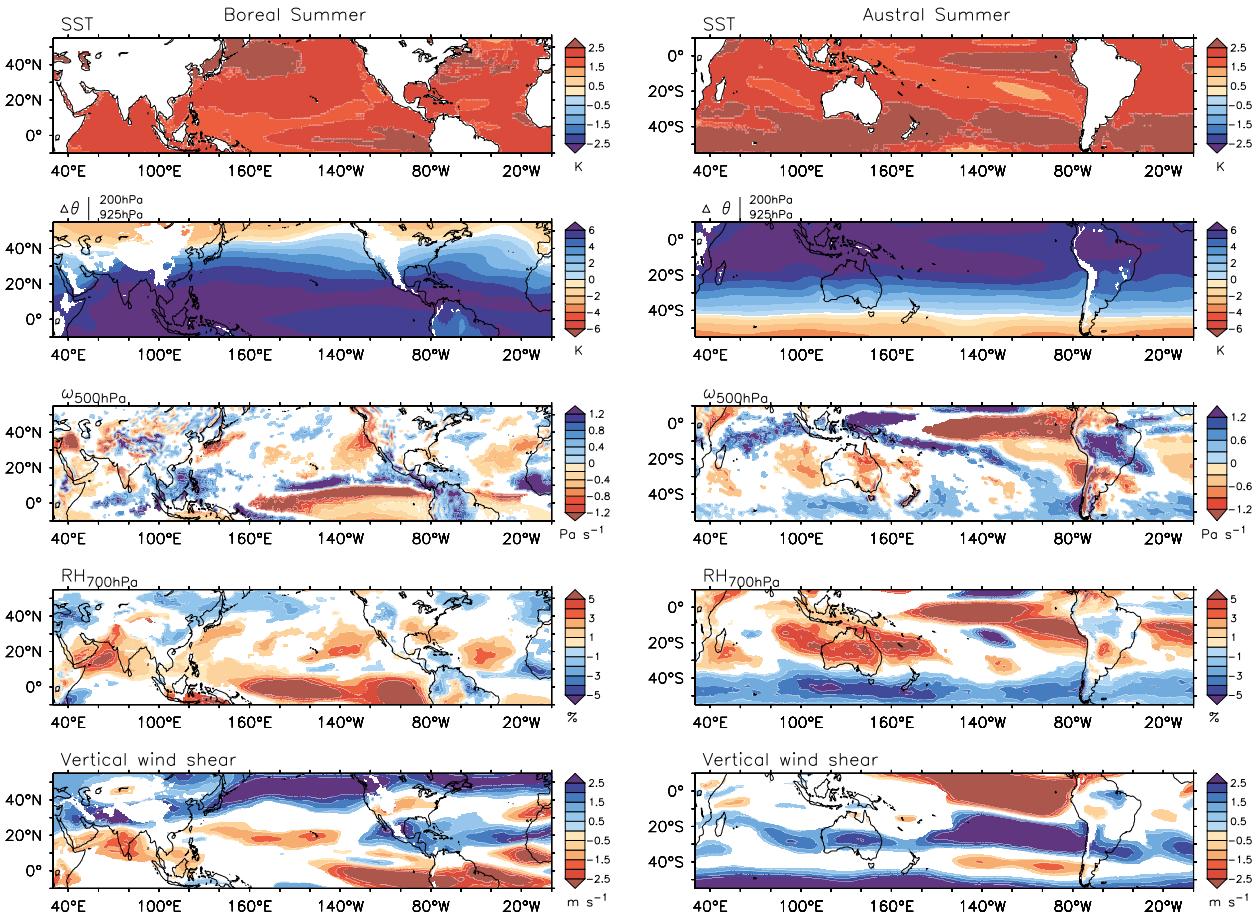

FIG. 11. Changes in large-scale environments between 2 × CO_2 and control simulations during summer for the (left) Northern and (right) Southern Hemisphere: SST (K), the difference of potential temperature between 200 and 925 hPa that characterizes the dry static stability in the troposphere ($\Delta\theta|_{925\,\mathrm{hPa}}^{200\,\mathrm{hPa}}$) (K), $\omega_{500\,\mathrm{hPa}}$ (Pa s^{-1}), $RH_{700\,\mathrm{hPa}}$ (%), and vertical wind shear between 200 and 850 hPa (m s^{-1}). Only statistically significant areas ($p < 0.1$) based on the two-sided Student's t test are drawn. The warm (cold) colors represent more (less) favorable conditions for TC activity.

occurrence are larger in percentage terms than for TC wind speed. In fact, the PDI per TC (not annually accumulated) has a marginal increase (+3.4% for the globe) in response to CO_2 doubling (Table 2). However, the annually accumulated PDI change remains negative (−3.5%) globally, due to the influence of reduced TC counts and lifetimes (Tables 1 and 2).

An important question concerning TCs and climate change is whether the observed correlation between low-frequency variations of basinwide Atlantic PDI and tropical Atlantic SST (Emanuel 2007) can be used to infer PDI changes due to radiatively forced climate change (e.g., Vecchi et al. 2008). The present results provide further support for the projection analysis of Vecchi et al. (2008) that suggests that the Atlantic basinwide PDI changes associated with global warming are not well described statistically by local tropical Atlantic SST changes alone.

f. *Large-scale environments*

To further explore the environmental factors influencing changes in TC activity, Fig. 11 shows the simulated changes in several such factors in response to a CO_2 doubling. Separate maps are shown for the Northern and Southern Hemisphere summers. As is well known, climate models consistently project that the SST will increase globally as the CO_2 concentration in the atmosphere increases (Solomon et al. 2007). In CM2.5, the SST increase for a CO_2 doubling is about 2.1 K over the tropical region (30°S–30°N). Meanwhile, the simulated tropical atmospheric warming is larger in the upper troposphere than near the surface, resulting in increased static stability over the TC formation regions. This increasing dry static stability in the tropical atmosphere under CO_2-induced warming is a common feature across IPCC AR4 global warming simulations (Solomon et al. 2007; Hill and

Lackmann 2011). The increasing static stability could inhibit the global TC formation through a decrease in the tropical overturning circulations (Bengtsson et al. 2007; Sugi et al. 2002), although the mechanisms for this process remain unclear (Knutson et al. 2010). Higher SSTs supply more energy for TCs to be intensified, although a more physically complete explanation also must consider concomitant changes in the tropical atmosphere (Emanuel 1987). The changes in these two factors (SST and dry static stability) take place over the whole domain of TC activity in both hemispheres. However, these two factors alone apparently cannot sufficiently explain the regional differences in TC response shown in Fig. 10.

Other possibly important environmental factors such as $\omega_{500\,\mathrm{hPa}}$, 700-hPa relative humidity $\mathrm{RH}_{700\,\mathrm{hPa}}$, and vertical wind shear show regionally varying responses to CO_2 doubling. The changes of $\omega_{500\,\mathrm{hPa}}$, reflecting changes in convective mass fluxes, may contribute to regional changes of TC genesis, as noted by Held and Zhao (2011). Positive changes of $\omega_{500\,\mathrm{hPa}}$ (i.e., anomalous mean descending motion) are simulated over the South China Sea, the Philippine Sea, parts of the North Indian Ocean, and from about 10° to 20°N in the central–eastern Pacific during boreal summer, and in the tropical South Indian and South Pacific Oceans during austral summer. Anomalous mean rising motion changes are simulated in the eastern Pacific for both seasons. On the other hand, the 700-hP relative humidity increases over the TC activity area for both hemispheres. The increase in relative humidity could induce increases in TC activity and TC size (Hill and Lackmann 2009) and enhancement of TC-induced rainfall rate (Jiang et al. 2008). The vertical wind shear during northern summer decreases over much of the tropics and subtopics in the North Pacific whereas it increases over the North Atlantic. As shown in Fig. 5, the vertical wind shear is statistically linked with the TC count over the NA basin and this linkage is also found for the long-term response to the CO_2 doubling.

The responses of $\omega_{500\,\mathrm{hPa}}$, $\mathrm{RH}_{700\,\mathrm{hPa}}$, and vertical wind shear to CO_2 doubling show more complicated spatial structure in their changed fields compared to the responses of SST and dry static stability. These factors are apparently responsible for modulating the model's response of TC activity to the CO_2 doubling at the regional (subbasin) scale. However, we could not find significant relationship between any single environmental parameter and TC response, suggesting the TC changes are a response to several large-scale environmental factors.

g. *On the issues in Atlantic TC response to warm climate*

Previous studies suggested that the "relative SST" over the Atlantic MDR has a strong statistical association with TC frequency in the NA basin (Zhao et al. 2009; Villarini et al. 2010, 2011; Vecchi et al. 2011). The relative SST here is defined as the difference between the area-averaged SST over the MDR ($\mathrm{SST}_{\mathrm{MDR}}$) and the SST averaged over the global tropics (here defined as 30°N–30°S). Using the statistical model developed by Villarini et al. (2011) for Atlantic TC counts, the relative SST changes simulated by CM2.5 imply a 10% reduction in Atlantic TC count during August–October in response to the CO_2 doubling, which is a smaller decrease than obtained directly from the CM2.5 dynamical projection (−30%). However, our results qualitatively support the notion that relative SST is an important predictor variable for Atlantic TC frequency changes—even those in response to a CO_2-induced global warming (Zhao et al. 2009; Knutson et al. 2013). It is notable that some dynamical models do not project a reduction of Atlantic TCs in a climate warming scenario (e.g., Sugi et al. 2002, 2009; Emanuel et al. 2008; Oouchi et al. 2006). However, as shown in Villarini et al. (2011) and Knutson et al. (2013), models that project an increased (decreased) Atlantic TC count usually have, or are being forced with, positive (negative) relative SST changes in the warmer climate.

Doi et al. (2013) found enhanced interannual variations of $\mathrm{SST}_{\mathrm{MDR}}$ during early boreal summer in a CO_2-warmed climate and suggested that the higher Atlantic TC counts could occur during warm $\mathrm{SST}_{\mathrm{MDR}}$ years with the warmer climate than during warm $\mathrm{SST}_{\mathrm{MDR}}$ years in the present climate, even if the mean Atlantic TC count were reduced overall. Because their TC inferences were derived from a statistical TC projection technique based on the relative SST, we reexamine this issue here based on the TC simulations in our dynamical model (i.e., CM2.5). Table 3 (top) shows, for both the control and $2 \times CO_2$ climate, the mean Atlantic TC count for all years and the increases in the count during warm $\mathrm{SST}_{\mathrm{MDR}}$ years. The warm $\mathrm{SST}_{\mathrm{MDR}}$ years are defined as years when the $\mathrm{SST}_{\mathrm{MDR}}$ is greater than one standard deviation over the climatological mean $\mathrm{SST}_{\mathrm{MDR}}$ for either the control or $2 \times CO_2$ runs. The results show that in the control simulation, Atlantic TC counts increase by 26% during warm $\mathrm{SST}_{\mathrm{MDR}}$ years, while in the $2 \times CO_2$ experiment the counts increase by 53% in warm $\mathrm{SST}_{\mathrm{MDR}}$ years. Thus, despite the decrease in mean TC count in the Atlantic (−30%) in the $2 \times CO_2$ run, the increase in TC counts during warm SST years is larger by 43% in the $2 \times CO_2$ run than in the control run.

A similar analysis applied to annual PDI for Atlantic TCs yields similar results to those for TC counts (Table 3, bottom). The deviation from the climatological mean of annual PDI for warm $\mathrm{SST}_{\mathrm{MDR}}$ years is enhanced more than 200% in the $2 \times CO_2$ run relative to the

TABLE 3. Mean Atlantic (top) TC count and (bottom) annual PDI ($10^7\,m^{-3}\,s^{-2}$) for all years and the mean anomaly for unusually warm years in the MDR, defined as years in which SST MDR anomalies exceed one std dev relative to the long-term control or $2 \times CO_2$ climatology. Statistically significant changes with the two-sided Student's t test are denoted by an asterisk (*) for $p < 0.01$.

	Mean TC count (A)	Anomalous TC count, warm SST_{MDR} years (B)	Change [100(B/A)] (%)
Control	2.7	+0.7	+25.9*
$2 \times CO_2$	1.9	+1.0	+52.6*
[($2 \times CO_2$) − control]	−0.8* (−29.6%)	+0.3 (+42.9%)	—
	Mean PDI (C)	Anomalous PDI for warm SST_{MDR} years (D)	Change [100(D/C)] (%)
Control	49.1	+5.1	+10.4
$2 \times CO_2$	44.9	+20.0	+44.5*
[($2 \times CO_2$) − control]	−5.2 (−10.6%)	+14.9 (+292.2%)	—

control run. The actual mean annual PDI for warm SST_{MDR} years also becomes larger in the $2 \times CO_2$ run ($64.9 \times 10^7\,m^{-3}\,s^{-2}$) than in the control run ($54.2 \times 10^7\,m^{-3}\,s^{-2}$). These results must be viewed with caution due to the large negative biases in the genesis number and intensity of strong TCs in the Atlantic basin control simulation. Nevertheless, the results from CM2.5 for TC count and PDI support the findings of Doi et al. (2013), which were based on statistical downscaling only.

5. Summary and discussion

In this study, we analyzed the TC activity simulated by the GFDL CM2.5 high-resolution coupled climate model. CM2.5 simulates globally aggregated TC activity fairly realistically, including the global TC frequency and seasonal cycle, although there are biases in regional TC activity. In the North Atlantic, too few TCs are simulated, which appears to be related to large-scale environmental biases in the simulation, including a cold bias in tropical Atlantic SST, anomalous downward motion over much of the basin, and excessive vertical wind shear in the model. Elsewhere in the tropics, TC simulation biases also appear to be related to large-scale biases in the environmental fields. These results suggest a path for improving the simulation skill for TC activity in the model by reducing the simulation biases in the large-scale environment.

CM2.5 shows a notable ability to simulate the variability of TC activity related to ENSO. Despite the biases in the regional climatological TC activity in CM2.5, a number of observed ENSO-induced regional changes in TC activity over the globe are well captured by the model, such as the eastward shift of TC occurrence over the northwestern Pacific and reduced TC occurrence over during the North Atlantic during El Niño. The encouraging simulation of the ENSO-related TC activity changes suggests that CM2.5 is a useful tool to explore the TC response to other large-scale environmental changes, such as those associated with global warming. Moreover, because ENSO is one of the most important factors affecting TC activity, CM2.5 is a good candidate model for developing long-term (from seasonal to decadal) prediction of the TC activity.

The response of TC activity in CM2.5 to global warming is evaluated here by comparing the control run with a $2 \times CO_2$ run. The results show a substantial reduction of global TC frequency (−19%) in response to CO_2 doubling. The lifetime-maximum TC intensity increases by +2.7% in response to CO_2 doubling. This pair of findings is consistent with most other current climate modeling studies of TC behavior under climate warming (e.g., Knutson et al. 2010). However, the TC intensity response of the model, in particular, to CO_2 doubling should be viewed with caution because this model has a clear deficiency in simulating very strong TCs, due at least in part to its coarse resolution compared to hurricane scales. With this caveat, the results provide some further support for the hypothesis that the frequency of the strongest TCs will increase in the twenty-first century due to climate warming, based on the shift of the intensity distribution toward higher maximum wind speeds in the $2 \times CO_2$ run. The increase in frequency of strong TCs may be a more important factor for future TC damage potential than the decrease in total TC frequency, since a large fraction of historical TC damage has been caused by a relatively few strong TCs (Mendelsohn et al. 2012; Pielke et al. 2008). However, assessing the damage potential implied by the changes in various TC characteristics is beyond the scope of our study.

We have examined other factors known to contribute to TC damages such as lifetime, track length, translation speed, and storm size. TC damage tends to be larger when the TC translation speed is slow (Mahendran 1998; Holland et al. 2010) and the TC size is large (Powell and

Reinhold 2007; Maclay et al. 2008). In response to a CO_2 doubling, we find significant decreases in the average lifetime and track length but no significant change in translation speed. The TC size (horizontal extent of strong surface winds) shows some statistically significant increases (from +2% to +4% depending on the size metric) in response to CO_2 doubling.

The TC rainfall rate, in response to CO_2 doubling, shows a significant increase over all basins, by about 8%–18% when averaged within a radius of 250 km from the TC center. This increase rate is broadly consistent with the previous studies [see Table S3 in Knutson et al. (2010); Knutson et al. (2013)]. The percent increase in TC rainfall rate roughly scales with the increase in water holding capacity of the troposphere under $2 \times CO_2$ (see also Knutson et al. 2013), at least over the Northern Hemisphere basins, although in the Southern Hemisphere basins the increase is less than implied by this simple scaling. The smaller response in the Southern Hemisphere is probably related to the smaller intensification of TCs in the Southern Hemisphere basins compared to the Northern Hemisphere. We interpret the results as suggestive of a role for TC intensification in modulating the TC rainfall response to global warming.

The responses of various TC characteristics to CO_2 doubling have a spatially inhomogeneous regional pattern (Fig. 10). In general, the TC occurrence and intensity tend to exhibit regional changes of opposite sign. That is, the two parameters have opposing tendencies but similar spatial patterns of response to CO_2 doubling. The annual PDI response pattern tends to follow more closely the TC occurrence response pattern due to a larger proportional change of TC occurrence compared to intensity.

The TC response to CO_2 doubling can be interpreted in terms of changes in environmental parameters. In response to CO_2 doubling, the simulated changes in SST and static stability have the same sign of change over the tropical region so they are good candidates to explain the relatively spatially homogenous changes in TC activity. On the other hand, the responses of vertical motion, relative humidity, and vertical wind shear to CO_2 doubling show more complicated spatial structure in their change fields. The spatially inhomogeneous changes in these factors may modulate the model's response of TC activity to CO_2 doubling at the subbasin scale. However, we could not isolate a significant relationship between the TC response and any single environmental parameter, suggesting the TC changes are a response to several of these environmental factors.

The decrease (−30%) in TC frequency simulated for the Atlantic basin under $2 \times CO_2$ is in qualitative agreement with the decrease (−10%) obtained using a statistical projection of relative MDR SST, which provides further support for the relative SST paradigm as a way of synthesizing and understanding differences between Atlantic basin TC projections from different studies and models. We also find that the fractional increase in TC count and PDI during anomalous warm years (due to interannual variability) is greater in the $2 \times CO_2$ climate than in the control climate. In other words, even though the climatological average PDI decreases in the $2 \times CO_2$ climate, the PDI increases so much during anomalously warm individual years that those highly active years are more active than the most active years in the control climate. This supports the suggestion by Doi et al. (2013) that the overall TC damage potential (aside from development and mitigation issues) may be elevated despite the reduced TC count in the Atlantic basin under $2 \times CO_2$ conditions. The topic of TC damage potential needs further study to include other possible influences even from the climate perspective, such as sea level rise and landfalling activity.

The CM2.5 experiments are distinct from experiments using an atmospheric GCM running over prescribed SSTs because CM2.5 can simulate many aspects of the atmosphere–ocean coupling processes. These processes are very important in TC development (e.g., Schade and Emanuel 1999; Bender and Ginis 2000), as well as in simulating the large-scale atmosphere–ocean circulations (e.g., Waliser et al. 1999; Douville 2004). Therefore, the question arises as to the influence of ocean coupling on the response of TC activity to global warming. One important process involving atmosphere–ocean interactions and TCs is the impact of the SST "cold wake" generated by the storm itself. In that regard, ocean coupling was assessed by Knutson et al. (2001) to have only a minor effect on the percent increase in TC intensity under climate warming. The effect of ocean coupling is examined in a different context in this study, as the ocean interacts with the changes in the atmosphere above it at all scales from the both the storm scale to the planetary scale. On the other hand, the storm-scale interaction is probably limited by the coarse grid and weaker than observed TCs in the model. Nonetheless, the large-scale interaction in CM2.5 adds an additional degree of realism beyond what one can obtain from the prescribed SST approach. Through the inclusion of more important processes in TC–climate change simulations, we are striving for a better understanding of this complex set of geophysical problems.

Acknowledgments. We thank the Willis Research Network for funding Hyeong-Seog Kim's participation in this project.

REFERENCES

Anderson, J. L., and Coauthors, 2004: The new GFDL global atmosphere and land model AM2-LM2: Evaluation with prescribed SST simulations. *J. Climate,* **17,** 4641–4673, doi:10.1175/JCLI-3223.1.

Bender, M. A., and I. Ginis, 2000: Real-case simulations of hurricane–ocean interaction using a high-resolution coupled model: Effects on hurricane intensity. *Mon. Wea. Rev.,* **128,** 917–946, doi:10.1175/1520-0493(2000)128<0917:RCSOHO>2.0.CO;2.

——, T. R. Knutson, R. E. Tuleya, J. J. Sirutis, G. A. Vecchi, S. T. Garner, and I. M. Held, 2010: Modeled impact of anthropogenic warming on the frequency of intense Atlantic hurricanes. *Science,* **327,** 454–458, doi:10.1126/science.1180568.

Bengtsson, L., M. Botzet, and M. Esch, 1996: Will greenhouse gas-induced warming over the next 50 years lead to higher frequency and greater intensity of hurricanes? *Tellus,* **48A,** 57–73, doi:10.1034/j.1600-0870.1996.00004.x.

——, K. I. Hodges, M. Esch, N. Keenlyside, L. Kornblueh, J.-J. Luo, and T. Yamagata, 2007: How may tropical cyclones change in a warmer climate? *Tellus,* **59A,** 539–561, doi:10.1111/j.1600-0870.2007.00251.x.

Broccoli, A. J., and S. Manabe, 1990: Can existing climate models be used to study anthropogenic changes in tropical cyclone climate? *Geophys. Res. Lett.,* **17,** 1917–1920, doi:10.1029/GL017i011p01917.

Camargo, S. J., and A. H. Sobel, 2005: Western North Pacific tropical cyclone intensity and ENSO. *J. Climate,* **18,** 2996–3006, doi:10.1175/JCLI3457.1.

——, K. A. Emanuel, and A. H. Sobel, 2007: Use of a genesis potential index to diagnose ENSO effects on tropical cyclone genesis. *J. Climate,* **20,** 4819–4834, doi:10.1175/JCLI4282.1.

Chavas, D. R., and K. A. Emanuel, 2010: A QuickSCAT climatology of tropical cyclone size. *Geophys. Res. Lett.,* **37,** L18816, doi:10.1029/2010GL044558.

Chu, P.-S., 2002: Large-scale circulation features associated with decadal variations of tropical cyclone activity over the central North Pacific. *J. Climate,* **15,** 2678–2689, doi:10.1175/1520-0442(2002)015<2678:LSCFAW>2.0.CO;2.

Delworth, T. L., and Coauthors, 2006: GFDL's CM2 global coupled climate models. Part I: Formulation and simulation characteristics. *J. Climate,* **19,** 643–674, doi:10.1175/JCLI3629.1.

——, and Coauthors, 2012: Simulated climate and climate change in the GFDL CM2.5 high-resolution coupled climate model. *J. Climate,* **25,** 2755–2781, doi:10.1175/JCLI-D-11-00316.1.

Doi, T., G. A. Vecchi, A. J. Rosati, and T. L. Delworth, 2012: Biases in the Atlantic ITCZ in seasonal–interannual variations for a coarse- and a high-resolution coupled climate model. *J. Climate,* **25,** 5494–5511, doi:10.1175/JCLI-D-11-00360.1.

——, ——, ——, and ——, 2013: Response to CO_2 doubling of the Atlantic hurricane main development region in a high-resolution climate model. *J. Climate,* **26,** 4322–4334, doi:10.1175/JCLI-D-12-00110.1.

Douville, H., 2004: Relevance of soil moisture for seasonal atmospheric predictions: Is it an initial value problem? *Climate Dyn.,* **22,** 429–446, doi:10.1007/s00382-003-0386-5.

Elsner, J. B., J. P. Kossin, and T. H. Jagger, 2008: The increasing intensity of the strongest tropical cyclones. *Nature,* **455,** 92–95, doi:10.1038/nature07234.

Emanuel, K. A., 1987: The dependence of hurricane intensity on climate. *Nature,* **326,** 483–485, doi:10.1038/326483a0.

——, 2005: Increasing destructiveness of tropical cyclones over the past 30 years. *Nature,* **436,** 686–688, doi:10.1038/nature03906.

——, 2007: Environmental factors affecting tropical cyclone power dissipation. *J. Climate,* **20,** 5497–5509, doi:10.1175/2007JCLI1571.1.

——, R. Sundararajan, and J. Williams, 2008: Hurricanes and global warming: Results from downscaling IPCC AR4 simulations. *Bull. Amer. Meteor. Soc.,* **89,** 347–367, doi:10.1175/BAMS-89-3-347.

Evan, A. T., and S. J. Camargo, 2011: A climatology of Arabian Sea cyclonic storms. *J. Climate,* **24,** 140–158, doi:10.1175/2010JCLI3611.1.

Goldenberg, S. B., and L. J. Shapiro, 1996: Physical mechanisms for the association of El Niño and West African rainfall with Atlantic major hurricane activity. *J. Climate,* **9,** 1169–1187, doi:10.1175/1520-0442(1996)009<1169:PMFTAO>2.0.CO;2.

Griffies, S. M., 2010: Elements of MOM4P1. GFDL Ocean Group Tech. Rep. 6, NOAA/Geophysical Fluid Dynamics Laboratory, 377 pp. [Available online at http://data1.gfdl.noaa.gov/~arl/pubrel/o/old/doc/mom4p1_guide.pdf.]

Gualdi, S., E. Scoccimarro, and A. Navarra, 2008: Changes in tropical cyclone activity due to global warming: Results from a high-resolution coupled general circulation model. *J. Climate,* **21,** 5204–5228, doi:10.1175/2008JCLI1921.1.

Haarsma, R. J., J. F. B. Mitchell, and C. A. Senior, 1993: Tropical disturbances in a GCM. *Climate Dyn.,* **8,** 247–257, doi:10.1007/BF00198619.

Held, I. M., and M. Zhao, 2011: The response of tropical cyclone statistics to an increase in CO_2 with fixed sea surface temperatures. *J. Climate,* **24,** 5353–5364, doi:10.1175/JCLI-D-11-00050.1.

Hill, K. A., and G. M. Lackmann, 2009: Influence of environmental humidity on tropical cyclone size. *Mon. Wea. Rev.,* **137,** 3294–3315, doi:10.1175/2009MWR2679.1.

——, and ——, 2011: The impact of future climate change on TC intensity and structure: A downscaling approach. *J. Climate,* **24,** 4644–4661, doi:10.1175/2011JCLI3761.1.

Holland, G. J., J. Done, C. Bruyere, C. Cooper, and A. Suzuki-Parker, 2010: Model investigations of the effects of climate variability and change on future Gulf of Mexico tropical cyclone activity. *2010 Offshore Technology Conf.,* Houston, TX, OTC, 20690. [Available online at http://www.netl.doe.gov/kmd/RPSEA_Project_Outreach/07121-DW1801_OTC-20690-MS.pdf.]

Jiang, H., J. B. Halverson, and E. J. Zipser, 2008: Influence of environmental moisture on TRMM-derived tropical cyclone precipitation over land and ocean. *Geophys. Res. Lett.,* **35,** L17806, doi:10.1029/2008GL034658.

Kanamitsu, M., W. Ebisuzaki, J. Woollen, S.-K. Yang, J. J. Hnilo, M. Fiorino, and G. L. Potter, 2002: NCEP–DOE AMIP-II Reanalysis (R-2). *Bull. Amer. Meteor. Soc.,* **83,** 1631–1643, doi:10.1175/BAMS-83-11-1631.

Klotzbach, P. J., 2011: The influence of El Niño–Southern Oscillation and the Atlantic multidecadal oscillation on Caribbean tropical cyclone activity. *J. Climate,* **24,** 721–731, doi:10.1175/2010JCLI3705.1.

Knapp, K. R., M. C. Kruk, D. H. Levinson, H. J. Diamond, and C. J. Neumann, 2010: The International Best Track Archive for Climate Stewardship (IBTrACS). *Bull. Amer. Meteor. Soc.,* **91,** 363–376, doi:10.1175/2009BAMS2755.1.

Knutson, T. R., R. E. Tuleya, and Y. Kurihara, 1998: Simulated increase of hurricane intensities in a CO_2-warmed climate. *Science,* **279,** 1018–1020, doi:10.1126/science.279.5353.1018.

——, ——, W. Shen, and I. Ginis, 2001: Impact of CO_2-induced warming on hurricane intensities simulated in a hurricane model with ocean coupling. *J. Climate,* **14,** 2458–2468, doi:10.1175/1520-0442(2001)014<2458:IOCIWO>2.0.CO;2.

——, and Coauthors, 2010: Tropical cyclones and climate change. *Nat. Geosci.,* **3,** 157–163, doi:10.1038/ngeo779.

——, and Coauthors, 2013: Dynamical downscaling projections of twenty-first-century Atlantic hurricane activity: CMIP3 and CMIP5 model-based scenarios. *J. Climate,* **26,** 6591–6617, doi:10.1175/JCLI-D-12-00539.1.

Kuleshov, Y., L. Qi, R. Fawcett, and D. Jones, 2008: On tropical cyclone activity in the Southern Hemisphere: Trends and the ENSO connection. *Geophys. Res. Lett.,* **35,** L14S08, doi:10.1029/2007GL032983.

Landsea, C. W., G. D. Bell, W. M. Gray, and S. B. Goldenberg, 1998: The extremely active 1995 Atlantic hurricane season: Environmental conditions and verification of seasonal forecasts. *Mon. Wea. Rev.,* **126,** 1174–1193, doi:10.1175/1520-0493(1998)126<1174:TEAAHS>2.0.CO;2.

Lin, S.-J., 2004: A ''vertically Lagrangian'' finite-volume dynamical core for global models. *Mon. Wea. Rev.,* **132,** 2293–2307, doi:10.1175/1520-0493(2004)132<2293:AVLFDC>2.0.CO;2.

Lock, A. P., A. R. Brown, M. R. Bush, G. M. Martin, and R. N. B. Smith, 2000: A new boundary layer mixing scheme. Part I: Scheme description and single-column model tests. *Mon. Wea. Rev.,* **128,** 3187–3199, doi:10.1175/1520-0493(2000)128<3187:ANBLMS>2.0.CO;2.

Maclay, K. S., M. DeMaria, and T. H. Vonder Haar, 2008: Tropical cyclone inner-core kinetic energy evolution. *Mon. Wea. Rev.,* **136,** 4882–4898, doi:10.1175/2008MWR2268.1.

Mahendran, M., 1998: Cyclone intensity categories. *Wea. Forecasting,* **13,** 878–883, doi:10.1175/1520-0434(1998)013<0878:CIC>2.0.CO;2.

Mendelsohn, R., K. Emanuel, S. Chonabayashi, and L. Bakkensen, 2012: The impact of climate change on global tropical cyclone damage. *Nat. Climate Change,* **2,** 205–209, doi:10.1038/nclimate1357.

Moorthi, S., and M. J. Suarez, 1992: Relaxed Arakawa–Schubert: A parameterization of moist convection for general circulation models. *Mon. Wea. Rev.,* **120,** 978–1002, doi:10.1175/1520-0493(1992)120<0978:RASAPO>2.0.CO;2.

Murakami, H., B. Wang, and A. Kitoh, 2011: Future change of western North Pacific typhoons: Projections by a 20-km-mesh global atmospheric model. *J. Climate,* **24,** 1154–1169, doi:10.1175/2010JCLI3723.1.

——, and Coauthors, 2012: Future changes in tropical cyclone activity projected by the new high-resolution MRI-AGCM. *J. Climate,* **25,** 3237–3260, doi:10.1175/JCLI-D-11-00415.1.

Nicholls, N., 1979: Possible method for predicting seasonal tropical cyclone activity in the Australian region. *Mon. Wea. Rev.,* **107,** 1221–1224, doi:10.1175/1520-0493(1979)107<1221:APMFPS>2.0.CO;2.

Oouchi, K., J. Yoshimura, H. Yoshimura, R. Mizuta, S. Kusunoki, and A. Noda, 2006: Tropical cyclone climatology in a global-warming climate as simulated in a 20 km-mesh global atmospheric model: Frequency and wind intensity analyses. *J. Meteor. Soc. Japan,* **84,** 259–276, doi:10.2151/jmsj.84.259.

Pielke, R. A., J. Gratz, C. W. Landsea, D. Collins, M. A. Saunders, and R. Musulin, 2008: Normalized hurricane damages in the United States: 1990–2005. *Nat. Hazards Rev.,* **9,** 29–42, doi:10.1061/(ASCE)1527-6988(2008)9:1(29).

Powell, M. D., and T. A. Reinhold, 2007: Tropical cyclone destructive potential by integrated kinetic energy. *Bull. Amer. Meteor. Soc.,* **88,** 513–526, doi:10.1175/BAMS-88-4-513.

Putman, W. M., and S.-J. Lin, 2007: Finite-volume transport on various cubed-sphere grids. *J. Comput. Phys.,* **227,** 55–78, doi:10.1016/j.jcp.2007.07.022.

Schade, L. R., and K. A. Emanuel, 1999: The ocean's effect on the intensity of tropical cyclones: Results from a simple coupled atmosphere–ocean model. *J. Atmos. Sci.,* **56,** 642–651, doi:10.1175/1520-0469(1999)056<0642:TOSEOT>2.0.CO;2.

Smith, T. M., R. W. Reynolds, T. C. Peterson, and J. Lawrimore, 2008: Improvements to NOAA's historical merged land-ocean surface temperature analysis (1880–2006). *J. Climate,* **21,** 2283–2296, doi:10.1175/2007JCLI2100.1.

Solomon, S., D. Qin, M. Manning, Z. Chen, M. Marquis, K. Averyt, M. M. B. Tignor, and H. L. Miller Jr., 2007: *Climate Change 2007: The Physical Science Basis.* Cambridge University Press, 996 pp.

Sugi, M., A. Noda, and N. Sato, 2002: Influence of the global warming on tropical cyclone climatology: An experiment with the JMA global model. *J. Meteor. Soc. Japan,* **80,** 249–272.

——, H. Murakami, and J. Yoshimura, 2009: A reduction in global tropical cyclone frequency due to global warming. *SOLA,* **5,** 164–167, doi:10.2151/sola.2009-042.

Vecchi, G. A., and B. J. Soden, 2007: Increased tropical Atlantic wind shear in model projections of global warming. *Geophys. Res. Lett.,* **34,** L08702, doi:10.1029/2006GL028905.

——, K. L. Swanson, and B. J. Soden, 2008: Whither hurricane activity? *Science,* **322,** 687, doi:10.1126/science.1164396.

——, M. Zhao, H. Wang, G. Villarini, A. Rosati, A. Kumar, I. M. Held, and R. Gudgel, 2011: Statistical–dynamical predictions of seasonal North Atlantic hurricane activity. *Mon. Wea. Rev.,* **139,** 1070–1082, doi:10.1175/2010MWR3499.1.

——, S. Fueglistaler, I. M. Held, T. R. Knutson, and M. Zhao, 2013: Impacts of atmospheric temperature trends on tropical cyclone activity. *J. Climate,* **26,** 3877–3891, doi:10.1175/JCLI-D-12-00503.1.

Villarini, G., G. A. Vecchi, and J. A. Smith, 2010: Modeling the dependence of tropical storm counts in the North Atlantic basin on climate indices. *Mon. Wea. Rev.,* **138,** 2681–2705, doi:10.1175/2010MWR3315.1.

——, ——, T. R. Knutson, M. Zhao, and J. A. Smith, 2011: North Atlantic tropical storm frequency response to anthropogenic forcing: Projections and sources of uncertainty. *J. Climate,* **24,** 3224–3238, doi:10.1175/2011JCLI3853.1.

Waliser, D. E., K.-M. Lau, and J.-H. Kim, 1999: The influence of coupled sea surface temperatures on the Madden–Julian oscillation: A model perturbation experiment. *J. Atmos. Sci.,* **56,** 333–358, doi:10.1175/1520-0469(1999)056<0333:TIOCSS>2.0.CO;2.

Walsh, K. J. E., M. Fiorino, C. W. Landsea, and K. L. McInnes, 2007: Objectively determined resolution-dependent threshold criteria for the detection of tropical cyclones in climate models and reanalyses. *J. Climate,* **20,** 2307–2314, doi:10.1175/JCLI4074.1.

Wang, B., and J. C. L. Chan, 2002: How strong ENSO events affect tropical storm activity over the western North Pacific. *J. Climate,* **15,** 1643–1658, doi:10.1175/1520-0442(2002)015<1643:HSEEAT>2.0.CO;2.

Wang, H., J.-K. E. Schemm, A. Kumar, W. Wang, L. Long, M. Chelliah, G. D. Bell, and P. Peng, 2009: A statistical forecast model for Atlantic seasonal hurricane activity based on the NCEP dynamical seasonal forecast. *J. Climate,* **22,** 4481–4500, doi:10.1175/2009JCLI2753.1.

Weatherford, C. L., and W. M. Gray, 1988: Typhoon structure as revealed by aircraft reconnaissance. Part I: Data analysis and climatology. *Mon. Wea. Rev.,* **116,** 1032–1043, doi:10.1175/1520-0493(1988)116<1032:TSARBA>2.0.CO;2.

Yoshimura, J., M. Sugi, and A. Noda, 2006: Influence of greenhouse warming on tropical cyclone frequency. *J. Meteor. Soc. Japan,* **84,** 405–428, doi:10.2151/jmsj.84.405.

Zhao, M., and I. M. Held, 2012: TC-permitting GCM simulations of hurricane frequency response to sea surface temperature anomalies projected for the late twenty-first century. *J. Climate,* **25,** 2995–3009, doi:10.1175/JCLI-D-11-00313.1.

——, ——, S.-J. Lin, and G. A. Vecchi, 2009: Simulations of global hurricane climatology, interannual variability, and response to global warming using a 50-km resolution GCM. *J. Climate,* **22,** 6653–6678, doi:10.1175/2009JCLI3049.1.

——, ——, and ——, 2012: Some counterintuitive dependencies of tropical cyclone frequency on parameters in a GCM. *J. Atmos. Sci.,* **69,** 2272–2283, doi:10.1175/JAS-D-11-0238.1.